Spatiotemporal Analysis of Cell Response to a Rigidity Gradient: A Quantitative Study Using Multiple Optical Tweezers

Myriam Allioux-Guérin,[†] Delphine Icard-Arcizet,[‡] Christiane Durieux,[†] Sylvie Hénon,[‡] François Gallet,[‡] Jean-Claude Mevel,[†] Marie-Jo Masse,[†] Marc Tramier,[†] and Maïté Coppey-Moisan[†*]

[†]Complexes Macromoléculaires en Cellules Vivantes, Institut Jacques Monod, Unité Mixte de Recherche 7592, Centre National de la Recherche Scientifique, Université Paris Diderot-Paris 7, Université Pierre et Marie Curie-Paris 6, 75251 Paris, France; and [‡]Laboratoire Matière et Système Complexes, Université Paris Diderot-Paris 7, Centre National de la Recherche Scientifique, 75205 Paris, France

ABSTRACT We investigate the dynamic response of single cells to weak and local rigidities, applied at controlled adhesion sites. Using multiple latex beads functionalized with fibronectin, and each trapped in its own optical trap, we study the reaction in real time of single 3T3 fibroblast cells to asymmetrical tensions in the tens of pN $\cdot$ μm^{-1} range. We show that the cell feels a rigidity gradient even at this low range of tension, and over time develops an adapted change in the force exerted on each adhesion site. The rate at which force increases is proportional to trap stiffness. Actomyosin recruitment is regulated in space and time along the rigidity gradient, resulting in a linear relationship between the amount of recruited actin and the force developed independently in trap stiffness. This time-regulated actomyosin behavior sustains a constant and rigidity-independent velocity of beads inside the traps. Our results show that the strengthening of extracellular matrix-cytoskeleton linkages along a rigidity gradient is regulated by controlling adhesion area and actomyosin recruitment, to maintain a constant deformation of the extracellular matrix.

INTRODUCTION

During morphogenesis, tissue remodeling, and carcinogenesis, cells are subjected to mechanical tensions. Accumulating evidence indicates that cells can respond to physical parameters such as substrate rigidity (1) and mechanical stress (2,3), and to topographic features of the extracellular matrix (ECM) (4). Cellular responses to these mechanical forces result in different behaviors, from cell-shape changes (5) in tissue patterning to cell migration (1), differentiation (6), proliferation, and even apoptosis (7). Intracellular forces are generated by the dynamic behavior of the cytoskeleton (especially actin filaments) and molecular motors. They sustain these different changes in cell shape and tissue patterning. Interestingly, it was shown that, ex vivo, cell migration is guided by the rigidity of the substrate (39), and that anisotropic rigidity at adhesion sites can induce directional epithelial growth along the direction of greatest rigidity (8). It is likely that cells can sense not only global ECM rigidity, but also a local in vivo rigidity gradient.

In the last few years, mechanotransduction was investigated ex vivo, mostly on a macroscopic scale, by modifying substrate rigidities or by applying forces on large areas of cells (2,9). Using polyacrylamide matrices, it was shown that many different cell types sense and react to substrate stiffness (10). Spreading cells on deformable gels, such as silicone rubbers (11), or a high-density array of microfabricated elastomeric pillars (12) lead to a quantification of tractions forces generated by cells on their ECM. A linear relationship appears between these forces and the substrate rigidity. This likely provides a way for continuous tissue geometry adaptation in response to deformations (13). However, most of these techniques use the same high rigidity range (~100 kPa or nN $\cdot$ μm^{-1}), leading to forces of several nN at the scale of a single contact. Other nonquantitative studies performed on less rigid materials such as collagen gels showed different and more physiological cell behavior (14). In particular, adhesion complexes have different morphologies and compositions in softer contexts (15). This finding underscores the importance of studying a cell's mechanical sensitivity in low-rigidity conditions. Moreover, almost all previous studies involved the whole-cell level, ignoring heterogeneity within a single cell and the need for a more local and dynamic approach (16).

To gain insights into how cells can sense and respond to a rigidity gradient ex vivo, we used a nanomanipulation system to apply local and weak external mechanical stimulations on single cells. Several questions are addressed with this system: how small are the stiffnesses that a cell can sense? How do cells adjust to a rigidity gradient applied to their cortex, and what is their spatiotemporal response at the molecular level?

To tackle these questions, micron-sized latex beads coated with fibronectin were applied on a single cell and trapped simultaneously, using multiple optical tweezers (17). Because each coated bead behaves locally as an adhesion site of different stiffness, this system enabled us to mimic a rigidity gradient applied locally to the cell cortex. By combining

Submitted April 3, 2008, and accepted for publication September 2, 2008.

*Correspondence: coppey@ijm.jussieu.fr

Editor: Herbert Levine.

0006-3495/09/01/0238/10 $2.00

doi: 10.1529/biophysj.108.134627

force measurements and fluorescently tagged cytoskeleton (CSK) molecules, we were able to quantify, in single cells, the temporal relationship between the amplitude of CSK modifications, the forces exerted on adhesion sites, and the external stiffness of the mimicked ECM. This quantitative study emphasizes the relevance of dynamics in cellular processes underlying force response and actomyosin recruitment, which are involved in sensing a rigidity gradient. Importantly, our work suggests that a spatiotemporal regulation of the forces developed at contacts results in maintaining a constant deformation of the ECM-CSK linkage under tension.

MATERIALS AND METHODS

Cell culture

National Institutes of Health 3T3 mouse fibroblasts (henceforth referred to as 3T3) were grown in Dulbecco's modified Eagle's medium (DMEM Gibco, Invitrogen, Carlsbad, CA), supplemented with 10% fetal calf serum (PAA Laboratories GmbH, Pasching, Austria) at 37°C in a 5% CO_2 atmosphere.

Plasmid and transfections

National Institutes of Health 3T3 cells were transfected with Nanofectin (PAA Laboratories) and observed for 24 h after transfection. The enhanced green fluorescence protein (EGFP)-actin was constructed by replacement of the coding sequence of enhanced yellow fluorescence protein (EYFP), using the *Bsr*G1 and *Nhe*I sites, with that of EGFP, using a pEGFP-C1 plasmid and a pEYFP-actin plasmid (Clontech, Palo Alto, CA).

To obtain the mCherry-actin plasmid, we transferred the mCherry coding sequence from pRSETB-Cherry (a generous gift of Dr. R. Tsien, University of California at San Diego, San Diego, CA) into a Clontech vector backbone pEGFP-C1, taking advantage of the similar termini of mCherry and EGFP (18), leading to a pCherry-C1. The mCherry coding sequence was then exchanged with EGFP within the pEGFP-actin plasmid, using the *Nde*I and *Bgl*II sites.

The EGFP nonmuscle myosin II A (EGFP-NMMIIA) was a generous gift of M. Sheetz (construct described elsewhere) (19). The EGFP-vinculin plasmid was a generous gift of B. Geiger (20). A stable cell line of NIH 3T3 expressing EGFP-actin was also used (a generous gift of C. Ballestrem) (21).

Inhibitors

To inhibit NMMII specifically in our cells, Blebbistatin (Calbiochem, San Diego, CA) was used at a concentration of 50 μM. Blebbistatin is a selective, cell-permeable inhibitor of myosin II. It inhibits the ATPase activity of NMMII, and prevents myosin II-dependent processes (22).

Particular care must be taken when using Blebbistatin in vivo. Blebbistatin is photoinactivated by blue light (488 nm), and can release free radicals that can damage cells (23). To prevent this phototoxicity and photoinactivation by Blebbistatin, the inhibitor was used only in cells transfected with mCherry-actin, and cell lighting was attenuated as much as possible. Cells were observed ~20 min after Blebbistatin treatment.

Bead preparation

We coated 2-μm-diameter carboxylated polystyrene beads (Polysciences Europe, Eppelheim, Germany) with $FNIII_{7-10}$, i.e., a fragment of fibronectin (FN) type III domain 7–10, or with the entire protein (FN from bovine plasma, Sigma, St. Louis, MO), according to the method described by Felsenfeld et al. (24). Briefly, FN is an ECM protein interacting specifically with integrins and known to induce adhesion-dependent signaling (25). Beads were coated with biotinylated bovine serum albumin, using a carbodiimide linkage. Beads were then incubated with avidin and finally with biotinylated $FNIII_{7-10}$ (a generous gift of F. Coussen) or with biotinylated FN at a concentration of 0.7 μg/mL. Beads were used within 12 h after preparation, to ensure maximum functionality. Different coatings with the entire or truncated protein yielded to the same cell response, but the percentage of effectively functional proteins seems lower with the entire FN.

Coating density was checked as described below. A calibrated amount of coated beads was loaded on a nitrocellulose membrane (Schleicher and Schuele Bioscience, Keene, NH) and detected using an anti-FN primary antibody (a gift of F. Coussen) and anti-rabbit-horse radish peroxydase second antibody (Sigma). Immunoreactive bands were visualized using enhanced chemoluminescence (ECL) detection (Pierce, Rockford, IL). The amount of FN or $FNIII_{7-10}$ on each bead was ~30,000 molecules, and the bead coating was determined to be quantitatively reproducible. In addition, the amount of active proteins was likely similar for different coatings, because no variation in efficiency of the integrin/CSK link activation was found from one experiment to another. Noncoated beads were used as a control of specificity in this activation.

Setup of multiple optical tweezers coupled to fluorescence microscopy

The multiforce optical tweezers setup was described earlier (17). Briefly, the trapping source was a Nd:Yag laser set at 1064 nm (J 40, Spectra Physics, Mountain View, CA). Two crossed Acousto Optical Deflectors (AODs) (AA Opto-Electronique, St. Rémy-les-Chevreuses, France) were used to scan a single laser beam, and multioptical traps were generated by time-sharing of the laser between several positions. By controlling the amount of time spent by the laser at each position, we could control and adjust the stiffness of each trap. The outgoing laser beam was then sent onto an inverted microscope (Axiovert 135, Zeiss, SAS, Le Pecq, France) to the focusing objective (Zeiss Neofluor 100× oil, NA 1.3).

The system was coupled to epifluorescence and transmission observations, using the same microscope and the same objective. Using two electrical shutters (Uniblitz, Rochester, NY), we successively retrieved transmission and fluorescence images, using a highly sensitive CCD camera (Cool Snap HQ, Roper Scientific, Trenton, NJ). Images were acquired using MetaVue software (Roper Scientific). The fluorescence corresponding to different tagged proteins was selected using one of the filter-set combinations: 475AF40 excitation filter/505DRLP dichroic beam-splitter/535AF45 emission filter (GFP); or 540AF30 excitation filter/570DRLP dichroic beam-splitter/5F5ALP emission filter (mCherry) (Omega Optical, Inc., Brattleboro, VT).

Trapping stiffness calibration

Trapping rigidities were calibrated by the drag-force method (26), as described previously (27). Briefly, the chamber containing trapped beads was mounted on an X-Piezo-driven stage. A controlled oscillating movement was applied to the chamber, and trapped bead movement was recorded using a fast camera. The bead displacement generated by the known drag-force gave access to the tweezers force, and thus to the tweezers stiffness. The rigidity values varied between 20 pN $\cdot$ μm^{-1} and 300 pN $\cdot$ μm^{-1} (leading to forces from 10 to 200 pN), depending on the number of traps, on the laser-sharing time defined by the AODs, and on total laser power.

Cell experiments

For assays, cells were plated on 32-mm noncoated glass slides, 24 h or 48 h before observation. The coverslip was mounted on a holder to reconstruct a petri dish that was inserted into the thermostated chamber of the microscope. During experiments, cells were kept in DMEM F12 medium without phenol red, without riboflavin, without vitamin B12, with 20 mM HEPES, and with stable L-glutamine (PAA Laboratories GmbH) supplemented with 0.5% fetal calf serum. The chamber and objective were maintained at 37°C by a thermostated holder.

Three or four coated beads trapped with different rigidities were locally attached to the dorsal cortex of 3T3 cells through the integrin/FN link. For the entire acquisition time, the laser was turned on. Bead behaviors and fluorescence evolution were retrieved by successively taking one transmission image followed by one fluorescence image every 30 s. For some experiments, only transmission images were taken every 5 s. Fluorescence acquisition time was set between 500 ms and 2 s, depending on transfection efficiency. Each experiment lasted from 1–30 min. To rule out the possibility of laser heating artifacts, we applied the laser directly onto cells. No protein recruitment, cell damage, or other events were observed.

Force measurements

Bead displacement inside a trap is attributable to forces developed by cells and applied on beads. In such quasistatic conditions, the force exerted by the cell on beads counterbalances the restraining trapping force. Inside a trap, the recall force F_{trap}, created by the optical tweezers on the bead, increases linearly with its displacement. It follows the harmonic relationship $F_{trap}(t) = \Delta r(t) * k_{trap}$, where $\Delta r(t)$ is the displacement of the bead, and k_{trap} is the calibrated stiffness of the trap. The radius of the trap action was determined to be ~1 μm. Beyond this distance, we think that beads escape the traps, and no recall forces are exerted on the beads any longer.

Image analysis

Image analysis and measurement were performed using Image J (Rasband software, W.S., Image J, National Institutes of Health, Bethesda, MD, http://rsb.info.nih.gov/ij/, 1997–2005). Bead position was determined using an Image J plug-in ("Analyze Particles") that finds a bead's center of mass. Bead displacement as a function of time $r(t)$ was then calculated and used to find the bead velocity. We fitted $r(t)$ accurately with WaveMetrics Igor Pro software (http://www.wavemetrics.com), using the Levenberg-Marquardt algorithm to realize a linear regression, giving us the beads' speed.

For all fluorescence experiments, only low-expressing cells were considered. To analyze fluorescence images, line-scan profiles were obtained using Image J. Whenever possible, the amount of fluorescence recruited around each bead was quantified by the integration of this fluorescence profile. Whenever necessary, a photobleaching correction was performed.

CSK/ECM reinforcement assay

We defined a criterion to study the strengthening of the link between ECM and CSK after bead-cell contact. We used a previously described criterion (28) according to which reinforcement could be characterized by a restraint of bead movement.

After beads were placed on the cell cortex and trapped during various times at different rigidities, the same laser trap was used to try pulling the bead back, repositioning the stage so that the bead was placed at the point of maximum force. The linkage of the bead to the cell was described as reinforced if the laser trap force was not able to displace the bead on the cell surface (i.e., if no displacement of more than ~100 nm was seen with the camera). Otherwise, the linkage was said not to be reinforced.

RESULTS AND DISCUSSION

Cells sense a rigidity gradient: local forces increase proportional to local stiffness

Fibronectin and/or $FNIII_{7-10}$ fragment-coated beads (FN-coated), placed on the cortex of single cells, are simultaneously trapped in optical tweezers with different stiffnesses, to mimic a rigidity gradient of the ECM between adhesion sites. When FN-coated beads are held on the lamella of NIH 3T3 fibroblasts using optical tweezers, a weak first link between the bead and the cell is created in a few seconds. During the first minutes, beads remain quite immobile inside the trap. Around 2 min after their application on cells, 60% of the beads start to display a directed movement, oriented from the leading edge toward the nucleus (Fig. 1, *A* and *B*, *inset*). The proportion of moving beads does not depend on initial trap stiffness. Even beads that were only laid on cells without being held by the laser trap displayed a directed movement with the same percentage.

The existence of a latency time likely arises from a delay to engage or activate the few integrin receptors localized on the lamella and the corresponding signaling pathways. Indeed, 80% of noncoated beads do not display a directed movement, which shows that bead movements are specific to the cell response through the FN/integrin complex. The radius of action of traps is limited to a value close to 1 μm. Therefore, we think that 90% of moving beads escaped the trap after a mean time of 8 min $\pm$ 1 min 30 s.

Previous results demonstrated that this movement is driven by the rearward actin flow present in the lamella, and depends on actomyosin contractility (29). We observed

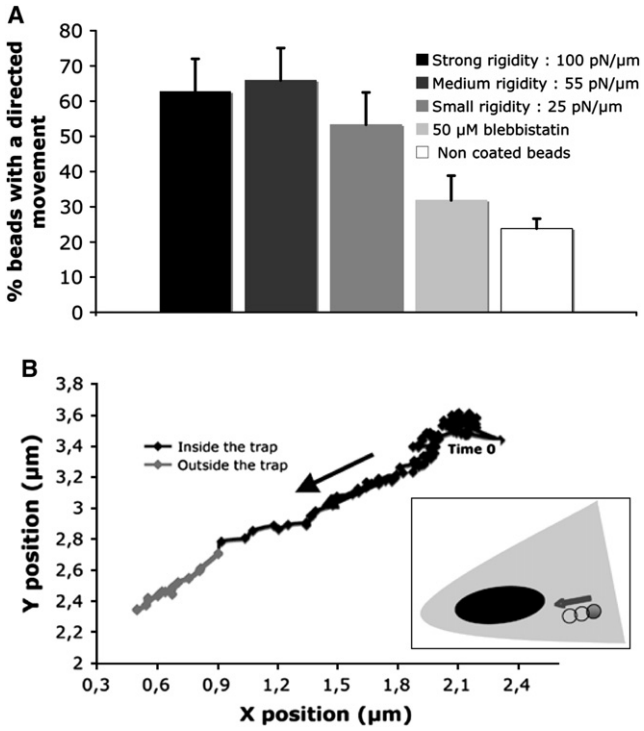

FIGURE 1 Actomyosin-dependent directed movement of trapped FN coated beads toward the nucleus. (*A*) Percentage of trapped beads displaying directed movement for three different trap stiffnesses (*black*, *dark-gray*, and *medium-gray columns*; measurements of 80 cells), in negative control condition (*open column*, trapped noncoated beads; measurements of 10 cells), and in the presence of 50 μM of Blebbistatin, a myosin II inhibitor (*light-gray column*; measurements of 23 cells). Results shown are the mean $\pm$ SD of at least three independent experiments. (*B*) On one cell, *X-Y* plot of one bead movement immediately after bead-cell contact. A certain time is necessary for the movement to install. (*Inset*) Schematic drawing of direction of bead movement on lamella of 3T3 cells.

that in the presence of Blebbistatin, a myosin II inhibitor, the percentage of beads displaying a directional movement was strongly diminished (from 60% to 30%; Fig. 1 *A*). The observed small remaining percentage of moving beads can be explained by two different hypotheses: 1), a nontotal inhibition of myosin II by Blebbistatin at 50 μM (30); and 2), partially rescued activity by another myosin (31,32).

Like traction forces exerted on their substrate, cells develop forces on the beads, pulling them away from the trap center. By recording bead displacements on a single cell and following the calculation described in the Materials and Methods section, we can retrieve the corresponding forces. We observe that the cell-bead forces increase with time, as beads move in the trap. We compared the temporal development of this force for three beads trapped with different stiffness on the same cell. Fig. 2 clearly shows a direct correlation between the trapping stiffness and the force evolution: the bead trapped with the strongest rigidity (~100 pN $\cdot$ μm^{-1}) is associated with the fastest force increase, whereas the bead trapped with the weakest rigidity (~25 pN $\cdot$ μm^{-1}) has a slower force evolution. The same profiles were observed and quantified in most cells. We demonstrate here that, at any time, a force proportional to the trap stiffness is developed by the cell.

Reinforcement of ECM/CSK link is time-regulated by trap stiffness and is myosin II-dependent

Choquet et al. showed that the ability of a cell to exert forces relies on the strengthening of the connection between the ECM and the cytoskeleton (28). External forces were shown to induce such a strengthening, but there is a lack of quantitative studies correlating the strengthening with local variations in ECM rigidity.

First, to explore the spatial resolution of the reinforcement, we placed two beads on a cell separated by a bead radius (2 μm). One bead was trapped, and the other was not. Eighty-five percent of the trapped beads, versus only 10% of the nontrapped beads, were reinforced. The strengthening of the ECM/CSK link took place only for trapped beads, and was localized to the area of increased tension.

Then three beads trapped with three different rigidities (100 pN $\cdot$ μm^{-1}, 55 pN $\cdot$ μm^{-1}, and 25 pN $\cdot$ μm^{-1}) were deposited on the lamella of single NIH 3T3 cells for different durations (1 min, 2 min, 3 min, and 15 min). The reinforcement was checked for each bead at the ends of the various trapping times. When the laser was applied for more than 10 min, most of the beads (>80%) displayed a reinforcement of the ECM/CSK link, regardless of trap stiffness, even for a rigidity as low as 20 pN $\cdot$ μm^{-1} (Fig. 3). The rigidity dependence of the reinforcement arose when laser traps were applied for <10 min. For 1-min trapping, the percentage of reinforced beads was 67%, with a rigidity of 100 pN $\cdot$ μm^{-1}, whereas no reinforcement was observed with a rigidity of 25 pN $\cdot$ μm^{-1}. Thus, a relationship appears to exist between the reinforcement time scale and the trapping rigidity.

In the presence of myosin II inhibitor, the percentage of reinforced beads was strongly diminished to 11%, versus 80% in control condition (Fig. 3). A small percentage of reinforcement was still observed: again, even though the level of myosin activity was strongly reduced, it was not completely suppressed by Blebbistatin, and we noticed an influence of rigidity on the reinforcement.

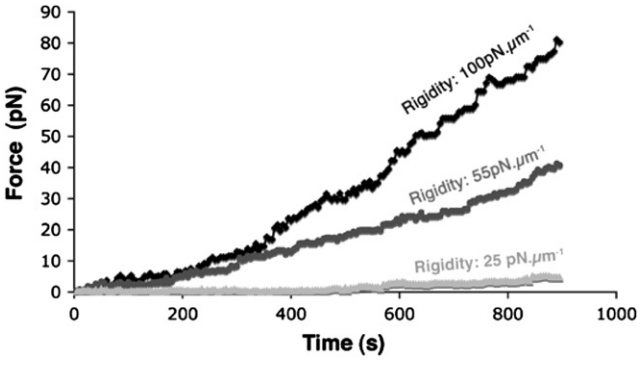

FIGURE 2 Cells respond to a rigidity gradient by developing local forces that increase in proportion to local rigidity. Plot is depicted of forces exerted by one cell on three beads trapped with different rigidities as a function of time. Corresponding optical tweezers stiffness values are indicated on curves. A typical experiment is shown here. The same results were obtained in 16 cells. The proportionality of the slope to the stiffness appears after a delay of 300 $\pm$ 100 s.

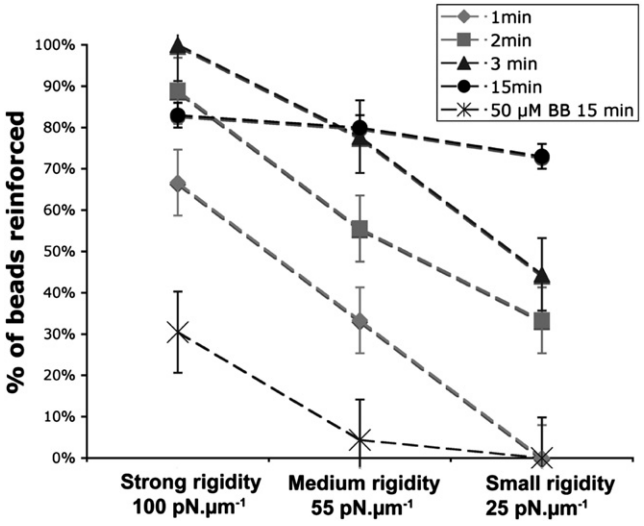

FIGURE 3 Reinforcement of ECM/CSK link is time-regulated by local trap stiffness. Percentage of beads corresponds to a reinforced ECM/CSK linkage as a function of trap stiffness and duration of laser application. Laser optical tweezers were applied for 15 min (*solid circles*, measurements of 80 cells), 3 min (*dark gray triangles*, measurements of eight cells), 2 min (*medium gray squares*, measurements of eight cells), and 1 min (*light gray diamonds*, measurements of six cells) in the absence of Blebbistatin, and for 15 min in the presence of 50 μM Blebbistatin (*black crosses*, measurements of 23 cells). Results are the mean $\pm$ SD of at least three independent experiments.

The ability of a cell to return to its initial state once the mechanical stimulus ends is essential. Relaxation processes inside the cell clearly contribute to the rapidity of a cellular response to mechanical environmental changes. Using the same reinforcement criterion, we studied the relaxation dynamics of the strengthened ECM/CSK links. But because the method used to check for reinforcement (i.e., bead-trapping by the laser) is a mechanical perturbation that could itself trigger reinforcement, we used twin beads (A and B) trapped together on the same cell lamella as duplicate systems supposed to have similar properties. Bead A was used to check, immediately after the 4-min trapping time, if the cell started a reinforcement process. This eliminated the 15% of cells that, on average, do not show any reinforcement. If bead A displayed reinforcement, we waited 8 min and checked the reinforcement on bead B. We assumed that if the contact at bead A was reinforced when the laser stopped, then statistically, the contact at bead B should also be reinforced. Hence relaxation was analyzed as the percentage of beads B displaying no reinforcement 8 min later: 90% of beads B exhibited this so-called relaxation 8 min after laser shutoff. This highlights the cell's ability to adapt quickly to mechanical changes.

Adhesion complex formation and actomyosin recruitment are regulated at a rate increasing with local rigidity

We monitored the reorganization of actin, NMMIIA, and vinculin in real time, during the application of a rigidity gradient on the 3T3 cell cortex, as shown in Figs. 4 and 5. After a mean time of 2 ± 1 min, we observed an accumulation of vinculin-GFP around the trapped beads. In some cases, this recruitment displayed the typical pattern of focal complexes, i.e., a small and elongated shape (33). In other cases, a more diffuse recruitment pattern was observed (Fig. 4 *A*). Vinculin was shown to be an indicator of a cell's ability to exert forces at adhesive contacts (34). Here, we observed that the amount of vinculin-GFP locally recruited increases with time (Fig. 4 *A*). It follows the same profile as the force developed on the

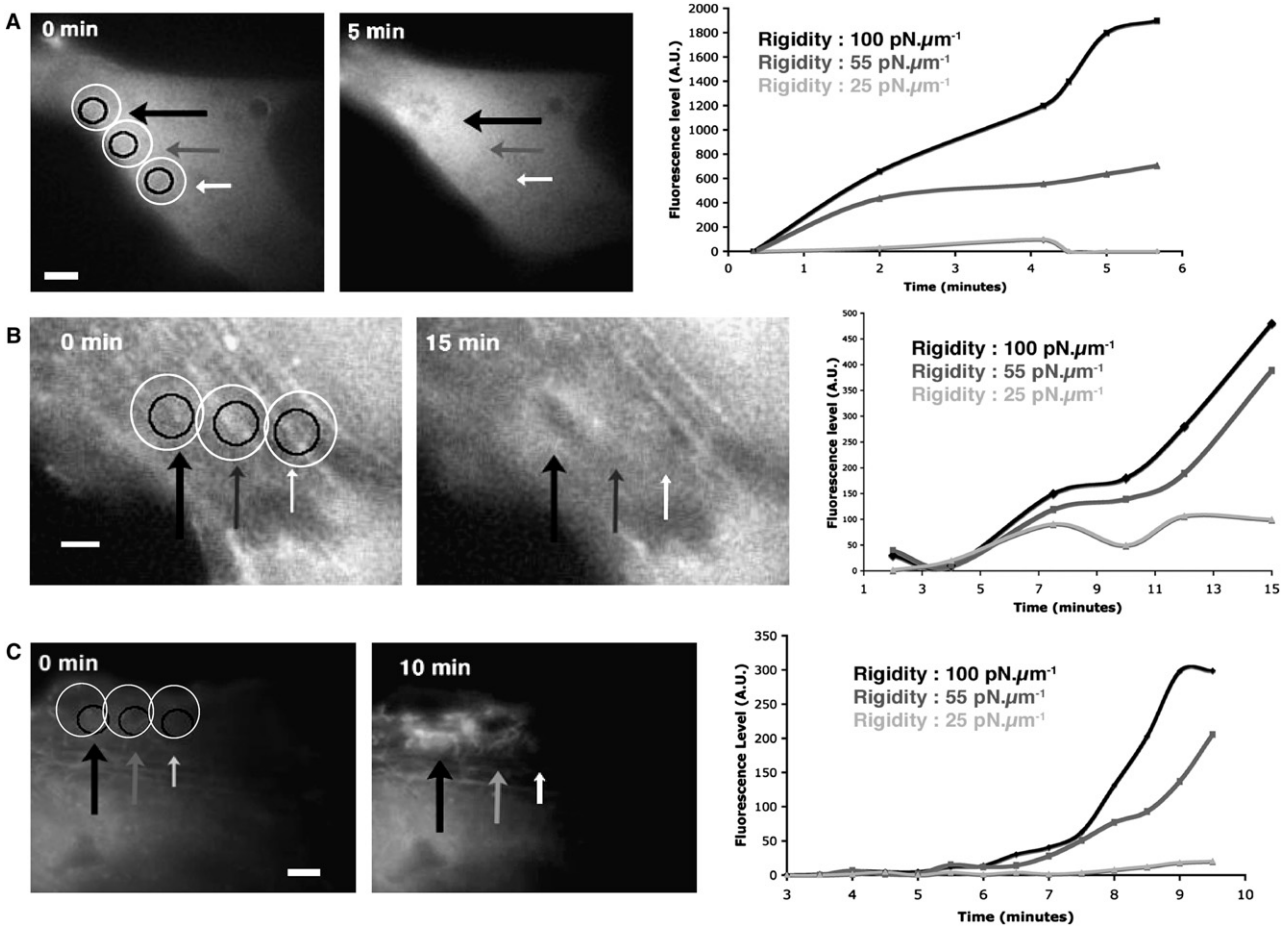

FIGURE 4 Focal complex development and actin recruitment around FN-coated beads are proportional to local rigidity. Epifluorescence images of 3T3 cell express vinculin-GFP (*A*) or actin-GFP (*B* and *C*) at the beginning (*left*) and at 5, 10, or 15 min (*middle*) after application of rigidity gradient. Rigidity gradient is visualized by size of arrows (*black*, 100 pN · μm^{-1}; dark gray, 55 pN · μm^{-1}; *light gray*, 25 pN · μm^{-1}). Bar, 2 μm. Graphs (*right*) represent the fluorescence intensity in the regions of interest (*white circles*) around each trapped bead (*black circles*) at different times after application of rigidity gradient.

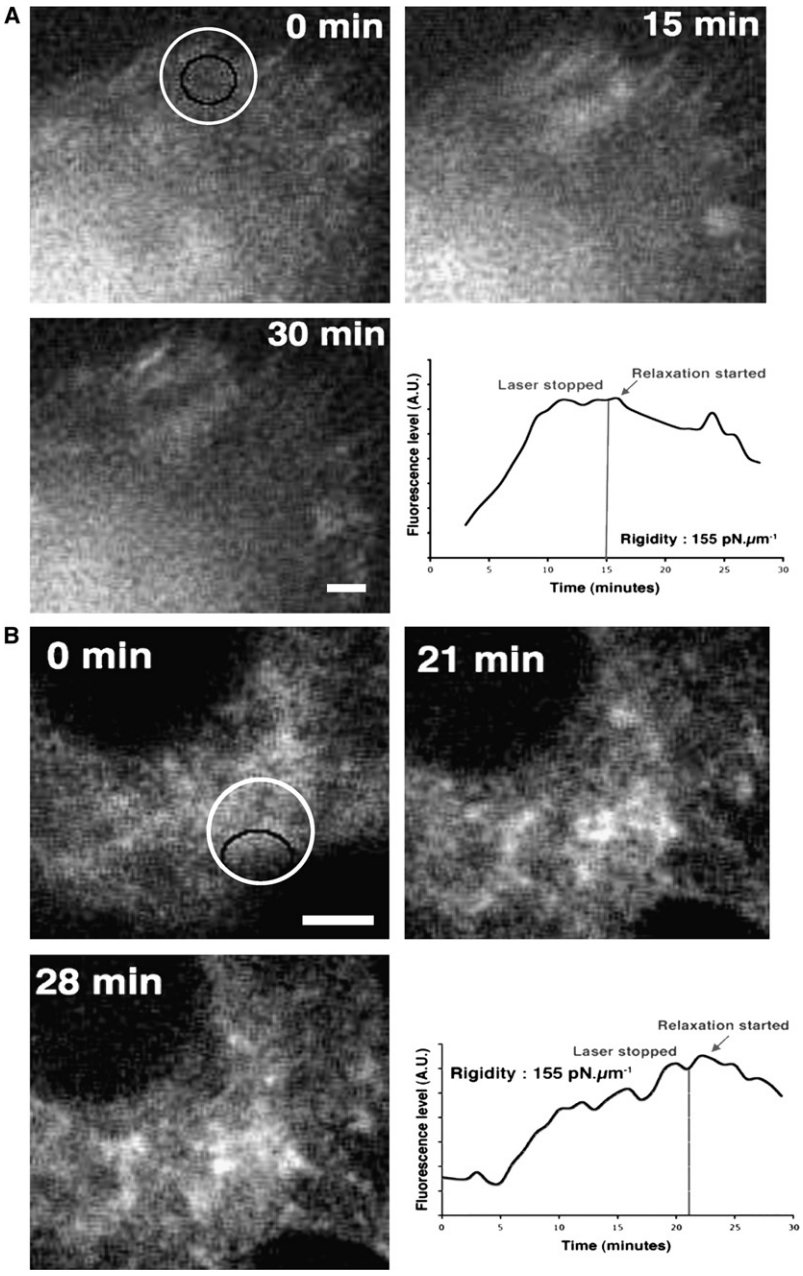

FIGURE 5 Actin and NMMIIA reorganization because of external tension is a reversible phenomenon. Epifluorescence images of 3T3 cells that express actin-GFP (*A*) and GFP-NMMIIA (*B*) around one trapped bead (trapping stiffness, 155 pN · μm^{-1}). At 15 min (*A*) and 21 min (*B*) after laser is stopped (*gray line on graph*), beads are no longer trapped. Graphs (*right*) represent fluorescence intensity in region of interest (*white circles*) around each trapped bead (*solid circles*) at different times after bead-cell contact. Bar, 2 μm.

corresponding trapped bead described above (Fig. 2), indicating that the total amount of vinculin-GFP is recruited proportionally to the trap stiffness.

After a mean value of 5.5 ± 1.5 min, actin-GFP was also reorganized beneath the cortical site where the trap was applied. It typically displayed two different patterns that were observed both independently and at the same time: 1), the appearance of new actin fibers and/or reinforcement of existing fibers; and 2), diffusely recruited actin. As for vinculin-GFP, the increase in amount of actin-GFP was proportional to the applied trap stiffness (Fig. 4, *B* and *C*).

To confirm that ECM stiffness regulates the organization not only of the actin CSK but of the entire actomyosin contractility network, we checked whether applying tensions onto cells led to myosin II reorganization. In 3T3 cells transfected with GFP-NMMIIA, we monitored the increase of GFP-NMMIIA fluorescence localized around the trapped beads, as described for GFP-actin. After 5–10 min on average, GFP-NMMIIA was reorganized around the beads. It displayed different typical patterns that were observed both independently or at the same time: 1), diffuse recruited myosin; 2), reinforcement of myosin patterns present at the beginning of the experiment; and 3), appearance of a semicircle of myosin fibers at a certain distance from the beads (3.5 ± 0.9 μm) (Fig. 5 *B*). Although less obvious than for actin or vinculin, myosin recruitment seemed to be proportional to

trap stiffness. For a stronger trap stiffness, a higher percentage of cells displayed visible myosin reorganization (62% for $k = 260$ pN $\cdot$ μm^{-1}, and 30% for $k = 40$ pN $\cdot$ μm^{-1}). Moreover, in the presence of 50 μM Blebbistatin, we never observed vinculin or actin recruitment.

To study the reversibility of actin recruitment, we switched off the laser after 15 min of bead-trapping. Switching off the laser led to a progressive loss of actin-GFP or GFP-NMMIIA around the beads in 75% of cells. The actin-GFP or GFP-NMMIIA decrease took place after a mean value of 5 $\pm$ 2.5 min (Fig. 5, *A* and *B*).

Nontrapped coated beads and trapped noncoated beads never displayed a local increase of fluorescence intensity, demonstrating the specific role played by FN and integrin activation in protein recruitment. Thus, mimicked ECM tensions induced locally the formation of adhesion complexes and the recruitment of actin and myosin. This recruitment, like the development of force, occurred even for very low tensions, at a rate proportional to local rigidity.

Cell forces and amount of actin at the contact: a linear relation independent of local rigidity

To analyze quantitatively the spatiotemporal relationship between the development of force and actin recruitment, we applied a rigidity gradient on the cell cortex, and at the same time we monitored bead displacements and actin-GFP fluorescence. Both the amplitude of force (F) and the amount of recruited actin-GFP (Q) increased in time. Fig. 6 shows a strong correlation, mainly linear, between the forces exerted by a single cell on each bead in its own optical trap and the localized GFP-actin fluorescence level around the bead (in total, 13 cells were studied; three examples are given in Fig. 6). The slope of the curve (F in function of Q) varied from cell to cell, but was independent of local rigidity for a given cell (Fig. 6).

The normalized fluorescence level of actin-GFP does not represent the total amount of actomyosin involved in the process. Endogenous nonfluorescent actin and myosin are not taken into account in the actin-recruitment quantification. Moreover, the proportion of fluorescent protein to the endogenous species is not known. This can at least partly explain the slope variation from cell to cell and the existence of an actin threshold in the force establishment for some cells (e.g., cell 3 in Fig. 6). Others parameters may play a role in this phenomenon, e.g., the variation of myosin activation in relation to local rigidities. This clearly highlights the validity of working with different rigidities on a single cell. Only this method can give quantitative results, because cell-to-cell variability strongly complicates comparisons in a whole-cell population.

Velocity of myosin-dependent retrograde actin flow under resisting forces is constant in time and independent of local trap rigidity

We quantified bead displacements as a function of time, to determine the velocity of their movement inside and outside

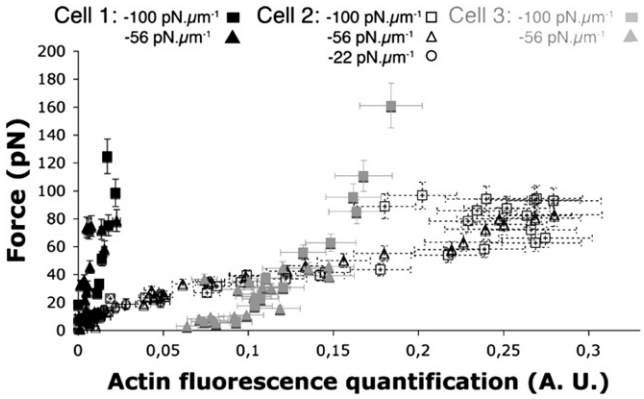

FIGURE 6 Linear relationship between cell-generated forces and actin recruitment, independent of local rigidity. Actin-GFP fluorescence and bead displacement were simultaneously followed on single cells during application of a rigidity gradient. The value of forces developed on each trapped bead is plotted as a function of the amount of locally recruited actin-GFP (fluorescence intensity in arbitrary units (A. U.); quantifications are described in Materials and Methods) for three different cells (*solid*, *open*, and *gray*). The same rigidity gradient was applied on three cells (three beads on each cell were trapped with rigidity values of 100 pN $\cdot$ μm^{-1}, 56 pN $\cdot$$\mu$m^{-1}, and 22 pN $\cdot$ μm^{-1}, *squares*, *triangles*, and *circles*, respectively). Cells 1 and 3 did not respond to weakest rigidity value of 22 pN $\cdot$ μm^{-1}. The relationship between force and recruited actin-GFP is mainly linear and independent of local trap rigidity.

the traps. Two regimes can be extracted for most trajectories (>75%; Fig. 7 *A*). The first regime (characterized by a constant velocity of 0.002 $\pm$ 0.0005 μm $\cdot$ s^{-1} after a delay of few minutes) corresponds to a bead displacement from the center of the trap to a mean distance of 0.9 $\pm$ 0.2 μm, and the second regime, after 0.9 $\pm$ 0.2 μm, is characterized by a constant velocity (0.007 $\pm$ 0.001 μm $\cdot$ s^{-1}), close to that of nontrapped beads (0.005 $\pm$ 0.0013 μm $\cdot$ s^{-1}). Consequently, the first velocity is likely to correspond to a restrained movement of the bead inside the trap, driven by retrograde actomyosin flow under a load. The second velocity corresponds to bead movement after escaping the trap, driven by retrograde actomyosin flow without a load. The displacement value at the transition between the two velocities, on the order of 1 μm, is consistent with the radius of action of our optical trap.

In the presence of Blebbistatin, a small percentage of beads still displayed directed movement (see previous section, Cell Forces and Amount of Actin at the Contact: A Linear Relation Independent of Local Rigidity section). The small percentage of beads that escaped the trap had the same biphasic trajectory profile as under normal conditions. The two characteristic velocities (0.001 $\pm$ 0.0001 μm $\cdot$ s^{-1} and 0.0046 $\pm$ 0.0001 μm $\cdot$ s^{-1}, respectively) measured were, however, significantly lower with Blebbistatin, especially inside the trap (Fig. 7 *B*). This slower retrograde flow is consistent with a reduced efficiency of actomyosin contractility.

Interestingly, the application of a rigidity gradient on the cell cortex reveals a rigidity-independent decrease of the

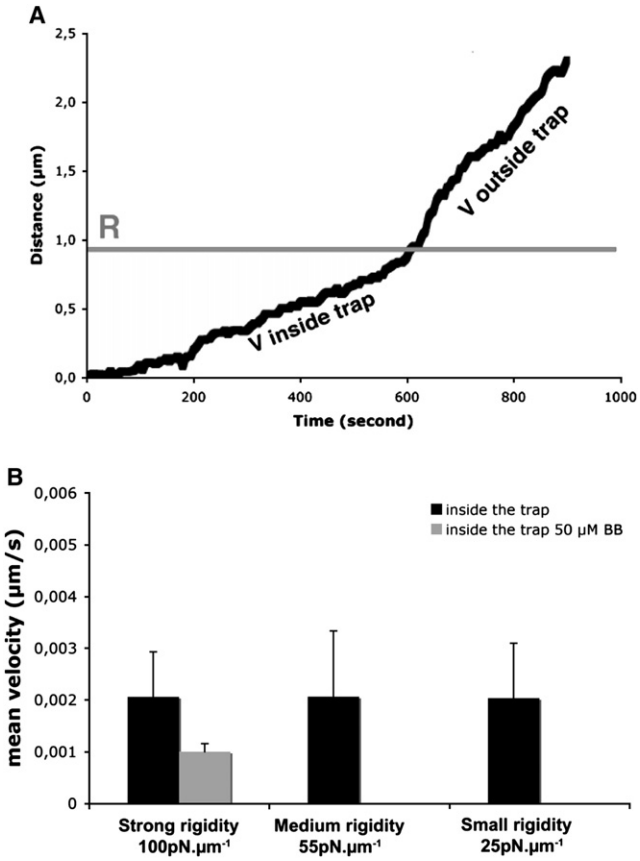

FIGURE 7 Bead velocity inside and outside traps: decrease of velocity of retrograde actomyosin flow under a load is a conserved parameter independent of local rigidity. (*A*) Plot of bead displacement versus time immediately after bead-cell contact. Gray line and *R* value represent limit between displacement inside trap and outside trap. A typical shape is depicted. Same results were obtained for each bead, whatever its trap rigidity, in 20 cells. (*B*) Average velocity of bead motion inside single traps for three different trap rigidities in the gradient, in the absence (*black*, measurements of 20 cells) and presence (*light gray*, measurements of five cells with strongest rigidity) of 50 μM Blebbistatin. Results shown are mean $\pm$ SD.

speed of the bead (Fig. 7, *B*). The bead velocity inside the trap is a conserved parameter of the cell response, independent of external stiffness. If we assumed a passive mechanism for bead displacement inside the trap, the bead should be slowed down, proportional to trap rigidity. Thus, the conservation of bead velocity along the rigidity gradient highlights the existence of a spatiotemporal cellular regulation controlling this velocity, i.e., the myosin-dependent retrograde actin flow. The fact that the velocity was conserved under a load means that the ECM deformations (Fig. 8, *d*) induced by the rigidity gradient were the same at any time.

A feedback loop links external tensions, actomyosin recruitment, and internal forces. By generalizing the force-velocity relationship for a single molecular motor to several motors acting cooperatively (see Eq. 2 in Supplementary Material), a constant velocity for the actomyosin retrograde flow under an increasing load can be obtained if the amount of recruited actomyosin increases linearly with the load, as already described. The cooperative behavior of actomyosin motors is thus critical for the response to a rigidity gradient. The molecular mechanisms that sustain the spatiotemporal regulation of forces developed by the cell on the adhesion sites are, however, not known. It would be interesting to determine the sensing mechanism that leads to a constant, rigidity-independent velocity of the actomyosin retrograde flow under a load. Cells precisely sense the restraining force on FN-coated beads (28). Is this force-sensing sufficient in itself to explain that the cellular response to a rigidity gradient is characterized by a rigidity-independent velocity of actomyosin retrograde flow under a load? By combining force-sensing features and the cooperative behavior of actomyosin motors, a theoretical model (Supplementary Material) provides quantitative predictions in agreement with our observations. Whatever the underlying sensing mechanism, a cell's answer to a rigidity gradient is a constant deformation of the ECM (Fig. 8).

CONCLUSIONS

We used multiple optical tweezers and FN-coated beads to mimic adhesion sites of fibroblast cells with an ECM. Our aim was to investigate quantitatively and in real time the cell's response to a rigidity gradient in the rigidity range of tens of pN $\cdot$ μm^{-1} (stresses of a few tens of Pa). Previous studies used deformable substrates to analyze, at the whole-cell level and at equilibrium, the relationship between ECM stiffness and cell contractility (11,12,35). Although the rigidity of these substrates can vary over a wide range, the lowest rigidity value is still about several tens of kPa, at the high end of in situ microenvironment rigidity, which can vary from 0.010–10 kPa (36,37).

The question, however, remains: how, in the lower part of this range, do cells respond quantitatively to a rigidity gradient? It was proved that fibroblasts can sense weak rigidities at their leading edge through a FN/integrin-dependent signaling (38), but it is not clear how the response is quantitatively related to rigidity in this range, or how cells discriminate between different rigidities at close adhesion sites.

Our choice of using multiple optical tweezers was motivated by the need to eliminate cell-to-cell variations and to perform quantitative analysis of time-dependent force establishment on the same cell.

We showed that single cells sense a rigidity gradient applied on their cortex by triggering a physiological response that is spatially and quantitatively resolved along the gradient. We characterize the spatiotemporal response in terms of internal forces, reinforcement, and amount of molecular reorganization. Beads are sensed in their own trap stiffness, even when they are close to each other. The forces exerted by a single cell on trapped beads increase with time, proportional to local rigidity. The time-increasing forces arise from time-regulated actomyosin contractility, as evidenced

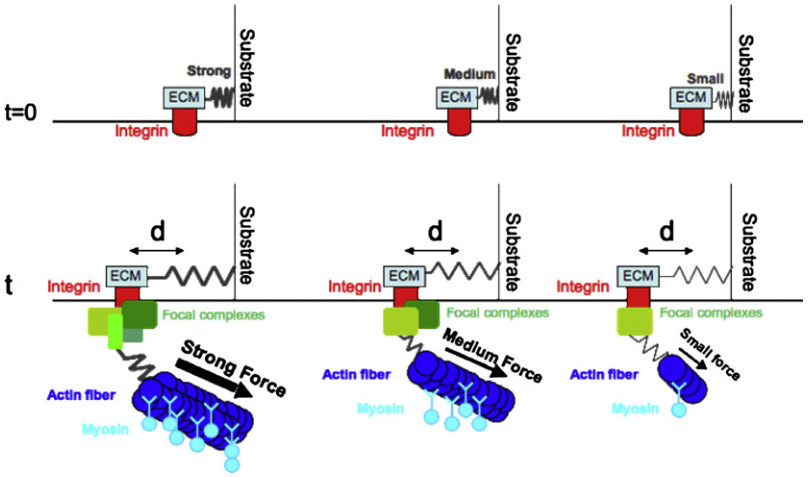

FIGURE 8 Spatiotemporal cellular response to an external rigidity gradient. The cartoon summarizes cellular response to a rigidity gradient applied on cell cortex with FN-coated beads simultaneously trapped with different stiffnesses (mimicking ECM rigidity gradient applied to adhesion sites). The movement of FN-coated beads (adhesion sites) is driven by myosin-dependent retrograde actin flow. The velocity of this flow is maintained constant along rigidity gradient, as long as beads stay in traps. This is attributable to regulated cooperative actomyosin recruitment that sustains an increase of force proportional to rigidity of ECM at adhesion sites. For strong (*left*), medium (*middle*), and weak (*right*) rigidity, deformation d of the external ECM substrate at time t remains the same.

by the time-increasing recruitment of actin and myosin IIA around trapped beads. Moreover, these recruitments, as well as force-driven bead movements, are strongly affected by the presence of Blebbistatin, suggesting a central role of myosin II in these processes.

We showed that the fibroblast response to a local stiffness as low as 20 pN $\cdot$ μm^{-1} involves molecular processes similar to those described for a stronger matrix stiffness (13). As visualized by the increase in vinculin-GFP fluorescence, adhesion complexes grow around the trapped bead, proportional to its own trap stiffness. Although performed in a weaker stiffness range, this finding is consistent with studies showing that stationary fibroblasts, spread on substrates of rigidity in the 10–20-kPa range, develop traction forces on focal adhesion sites proportional to the area of focal adhesion (34).

Interestingly, the spatiotemporal regulation of the cell response to a rigidity gradient is characterized by a linear relationship between the force generated on the trapped bead and the amount of locally recruited actin. This relationship is independent of local trap rigidity. In conjunction with this result, the rigidity and time independence of bead velocity inside the trap means that a rigidity-dependent and time-dependent regulation of actomyosin contractility takes place. We describe the theoretical rate of actomyosin recruitment as a function of the force developed at the contact by an empirical model, introducing the force-velocity relationship of several motors acting cooperatively. The underlying force-sensing assumption of the model is consistent with the fact that the time-dependence of reinforcement of the ECM-CSK link is regulated by local trap rigidity. Is this force-sensing, however, the only regulatory mechanism? The possibility cannot be excluded that the cell develops velocity-sensing and/or deformation-sensing to regulate the velocity of actomyosin retrograde flow under a load to a constant value.

Whatever the sensing mechanism, cells dynamically respond to a rigidity gradient by keeping a constant velocity of rearward actomyosin flow at contacts with the ECM. Thus, our results suggest a spatiotemporal regulation of actomyosin contractility, to maintain a constant deformation of the ECM at the level of adhesion sites, as schematized in Fig. 8.

We demonstrate the importance, not only of the global cellular sensing of matrix rigidity, but also of a local response to a mechanical gradient in the small rigidity range. This could help refine our knowledge of cell migration, adhesion, and polarization.

SUPPLEMENTARY MATERIAL

Modeling and equations are available at http://www.biophysj.org/biophysj/supplemental/S0006-3495(08)00018-0.

The authors thank Sergi Padilla (Institut Jacques Monod) and Terence Strick (Institut Jacques Monod) for critical reading of the manuscript and for very helpful advice, and Allison Marty (Pasteur Institute) for helping to improve the manuscript.

This work was supported by a grant from the Association pour la Recherche sur le Cancer, from Gefluc, and from the Agence National pour le Recherche (contracts 5A0631 and 5A0614).

REFERENCES

1. Pelham, R. J., Jr., and Y. Wang. 1997. Cell locomotion and focal adhesions are regulated by substrate flexibility. *Proc. Natl. Acad. Sci. USA.* 94:13661–13665.
2. Riveline, D., E. Zamir, N. Q. Balaban, U. S. Schwarz, T. Ishizaki, et al. 2001. Focal contacts as mechanosensors: externally applied local mechanical force induces growth of focal contacts by an mDia1-dependent and ROCK-independent mechanism. *J. Cell Biol.* 153:1175–1186.
3. Icard-Arcizet, D., O. Cardoso, A. Richert, and S. Henon. 2008. Cell stiffening in response to external stress is correlated to actin recruitment. *Biophys. J.* 94:2906–2913.
4. Thery, M., A. Pepin, E. Dressaire, Y. Chen, and M. Bornens. 2006. Cell distribution of stress fibres in response to the geometry of the adhesive environment. *Cell Motil. Cytoskeleton.* 63:341–355.
5. Engler, A., L. Bacakova, C. Newman, A. Hategan, M. Griffin, et al. 2004. Substrate compliance versus ligand density in cell on gel responses. *Biophys. J.* 86:617–628.

6. Engler, A. J., S. Sen, H. L. Sweeney, and D. E. Discher. 2006. Matrix elasticity directs stem cell lineage specification. *Cell.* 126:677–689.
7. Yeung, T., P. C. Georges, L. A. Flanagan, B. Marg, M. Ortiz, et al. 2005. Effects of substrate stiffness on cell morphology, cytoskeletal structure, and adhesion. *Cell Motil. Cytoskeleton.* 60:24–34.
8. Saez, A., M. Ghibaudo, A. Buguin, P. Silberzan, and B. Ladoux. 2007. Rigidity-driven growth and migration of epithelial cells on microstructured anisotropic substrates. *Proc. Natl. Acad. Sci. USA.* 104:8281–8286.
9. Galbraith, C. G., R. Skalak, and S. Chien. 1998. Shear stress induces spatial reorganization of the endothelial cell cytoskeleton. *Cell Motil. Cytoskeleton.* 40:317–330.
10. Wong, J. Y., J. B. Leach, and X. Q. Brown. 2004. Balance of chemistry, topography, and mechanics at the cell–biomaterial interface: issues and challenges for assessing the role of substrate mechanics on cell response. *Surf. Sci.* 570:119–133.
11. Lee, J., M. Leonard, T. Oliver, A. Ishihara, and K. Jacobson. 1994. Traction forces generated by locomoting keratocytes. *J. Cell Biol.* 127:1957–1964.
12. du Roure, O., A. Saez, A. Buguin, R. H. Austin, P. Chavrier, et al. 2005. Force mapping in epithelial cell migration. *Proc. Natl. Acad. Sci. USA.* 102:2390–2395.
13. Saez, A., A. Buguin, P. Silberzan, and B. Ladoux. 2005. Is the mechanical activity of epithelial cells controlled by deformations or forces? Biophys. J. 89:L52–L54.
14. Georges, P.C., and P.A. Janmey. 2005. Cell type-specific response to growth on soft materials. Am. Physiol. Soc. 1547–1553.
15. Cukierman, E., R. Pankov, D. R. Stevens, and K. M. Yamada. 2001. Taking cell-matrix adhesions to the third dimension. *Science.* 294:1708–1712.
16. Janmey, P. A., and D. A. Weitz. 2004. Dealing with mechanics: mechanisms of force transduction in cells. *Trends Biochem. Sci.* 29:364–370.
17. Emiliani, V., D. Sanvitto, M. Zahid, F. Gerbal, and M. Coppey-Moisan. 2004. Multi force optical tweezers to generate gradients of forces. *Opt. Express.* 12:3906–3910.
18. Tramier, M., M. Zahid, J. C. Mevel, M. J. Masse, and M. Coppey-Moisan. 2006. Sensitivity of CFP/YFP and GFP/mCherry pairs to donor photobleaching on FRET determination by fluorescence lifetime imaging microscopy in living cells. *Microsc. Res. Tech.* 69:933–939.
19. Meshel, A. S., Q. Wei, R. S. Adelstein, and M. P. Sheetz. 2005. Basic mechanism of three-dimensional collagen fibre transport by fibroblasts. *Nat. Cell Biol.* 7:157–164.
20. Zamir, E., B. Z. Katz, S. Aota, K. M. Yamada, B. Geiger, et al. 1999. Molecular diversity of cell-matrix adhesions. *J. Cell Sci.* 112:1655–1669.
21. Ballestrem, C., B. Wehrle-Haller, and B. A. Imhof. 1998. Actin dynamics in living mammalian cells. *J. Cell Sci.* 111:1649–1658.
22. Kovacs, M., J. Toth, C. Hetenyi, A. Malnasi-Csizmadia, and J. R. Sellers. 2004. Mechanism of Blebbistatin inhibition of myosin II. *J. Biol. Chem.* 279:35557–35563.
23. Sakamoto, T., J. Limouze, C. A. Combs, A. F. Straight, and J. R. Sellers. 2005. Blebbistatin, a myosin II inhibitor, is photoinactivated by blue light. *Biochemistry.* 44:584–588.
24. Felsenfeld, D. P., P. L. Schwartzberg, A. Venegas, R. Tse, and M. P. Sheetz. 1999. Selective regulation of integrin–cytoskeleton interactions by the tyrosine kinase Src. *Nat. Cell Biol.* 1:200–206.
25. Ruoslahti, E. 1988. Fibronectin and its receptors. *Annu. Rev. Biochem.* 57:375–413.
26. Svoboda, K., and S. M. Block. 1994. Biological applications of optical forces. *Annu. Rev. Biophys. Biomol. Struct.* 23:247–285.
27. Balland, M., N. Desprat, D. Icard, S. Fereol, A. Asnacios, et al. 2006. Power laws in microrheology experiments on living cells: comparative analysis and modeling. *Phys. Rev. E Stat. Nonlin. Soft Matter Phys.* 74:021911.
28. Choquet, D., D. P. Felsenfeld, and M. P. Sheetz. 1997. Extracellular matrix rigidity causes strengthening of integrin-cytoskeleton linkages. *Cell.* 88:39–48.
29. Caspi, A., O. Yeger, I. Grosheva, A. D. Bershadsky, and M. Elbaum. 2001. A new dimension in retrograde flow: centripetal movement of engulfed particles. *Biophys. J.* 81:1990–2000.
30. Straight, A. F., A. Cheung, J. Limouze, I. Chen, N. J. Westwood, et al. 2003. Dissecting temporal and spatial control of cytokinesis with a myosin II Inhibitor. *Science.* 299:1743–1747.
31. Maniak, M. 2001. Cell adhesion: ushering in a new understanding of myosin VII. *Curr. Biol.* 11:R315–R317.
32. Bershadsky, A. D., N. Q. Balaban, and B. Geiger. 2003. Adhesion-dependent cell mechanosensitivity. *Annu. Rev. Cell Dev. Biol.* 19:677–695.
33. Izzard, C. S. 1988. A precursor of the focal contact in cultured fibroblasts. *Cell Motil. Cytoskeleton.* 10:137–142.
34. Balaban, N. Q., U. S. Schwarz, D. Riveline, P. Goichberg, G. Tzur, et al. 2001. Force and focal adhesion assembly: a close relationship studied using elastic micropatterned substrates. *Nat. Cell Biol.* 3:466–472.
35. Wang, H. B., M. Dembo, and Y. L. Wang. 2000. Substrate flexibility regulates growth and apoptosis of normal but not transformed cells. *Am. J. Physiol. Cell Physiol.* 279:C1345–C1350.
36. Bao, G., and S. Suresh. 2003. Cell and molecular mechanics of biological materials. *Nat. Mater.* 2:715–725.
37. Discher, D. E., P. Janmey, and Y. L. Wang. 2005. Tissue cells feel and respond to the stiffness of their substrate. *Science.* 310:1139–1143.
38. Jiang, G., A. H. Huang, Y. Cai, M. Tanase, and M. P. Sheetz. 2006. Rigidity sensing at the leading edge through alphavbeta3 integrins and RPTPalpha. *Biophys. J.* 90:1804–1809.
39. Lo, C. M., H. B. Wang, M. Dembo, and Y. L. Wang. 2000. Cell movement is guided by the rigidity of the subtrate. *Biophys. J.* 79:144–152.